ELSEVIER

Polymer 41 (2000) 8363–8373

polymer

www.elsevier.nl/locate/polymer

Fracture of glass bead/epoxy composites: on micro-mechanical deformations

J. Lee[1,a], A.F. Yee[a, b,*]

[a]*Macromolecular Science and Engineering Center, The University of Michigan, Ann Arbor, MI 48109, USA*
[b]*Department of Materials Science and Engineering, The University of Michigan, Ann Arbor, MI 48109, USA*

Received 2 December 1999; received in revised form 24 February 2000; accepted 24 February 2000

Abstract

To understand the fracture behavior of inorganic particle filled polymers, glass bead filled epoxies having different glass bead contents and sizes were prepared as model systems. Although their macroscopic fracture behavior was brittle, diffuse matrix shear yielding and micro-shear banding were found to occur around crack paths. Besides these plastic deformations, debonding of glass beads, step formation on fracture surface, and birefringence due to thermal residual misfit between glass beads and matrix were identified and studied. The fracture toughness and modulus of composites generally increased with increase in the volume fraction of glass beads. Micro-shear band zone size, debonding zone size, and the areal density of steps also followed increases in the volume fraction. The effect of glass bead size on fracture toughness and modulus was not significant, but the areal density of steps was found to increase as the size decreased. Differential thermal contraction between glass beads and matrix was found to cause the thermal residual misfit, resulting in birefringence around glass beads. Microscopy studies revealed that this thermal residual misfit might not have an extensive influence on crack propagation. © 2000 Published by Elsevier Science Ltd.

Keywords: Fracture; Epoxies; Shear yielding

1. Introduction

Recently, interest in inorganic particle filled polymers is increasing again, mainly because their applications as electronic packaging and dental restoratives [1,2] are expanding. Understanding the effect of inorganic particle inclusion on the mechanical properties of resulting composites is essential for designing filled composites. Moreover, as a starting point for the study on newly developed inorganic–organic hybrid materials, the study on inorganic particle filled polymers is important. By increasing our understanding on this subject, we may be able to design composites with both rigidity and toughness [3].

Among the various modifications of mechanical properties by inorganic particle inclusion [3], the toughening and strengthening of polymers are the most important. In this study, the improvement of fracture toughness will be the main subject, as this is more challenging and less understood than the modification of other properties. The ultimate objective of our research is to understand the underlying mechanisms of inorganic particle toughening and utilize this understanding for the development of new toughened and stiffened composite materials. As the first attempt to achieve this objective, the effect of two basic material variables, volume fraction and size of glass beads, on the fracture toughness of composites will be explored.

The effects of volume fraction and size of glass beads on fracture behavior have been studied for a long time and are usually explained using the crack front bowing theory [3–12]. In most of the previous studies, three general trends can be found. Firstly, as the volume fraction of glass beads increases, the fracture toughness of composites (either critical stress intensity factor or strain energy release rates) increases. Secondly, the incremental toughening effect diminishes with increasing volume fraction. Thirdly, generally larger particle filled epoxies were slightly tougher than smaller particle filled epoxies, but the size effect is found to be of secondary influence on fracture toughness. Despite these studies, a detailed microscopy study of the fracture behavior corresponding to increasing the volume fraction

* Corresponding author. Fax: + 1-734-763-4788.
E-mail addresses: jong@cems.umn.edu (J. Lee), afyee@engin.umich.edu (A.F. Yee).
[1] Present address: Department of Chemical Engineering and Materials Science, University of Minnesota, Minneapolis, MN 55455, USA.

0032-3861/00/$ - see front matter © 2000 Published by Elsevier Science Ltd.
PII: S0032-3861(00)00187-7

Table 1
Designation of glass beads used in this experiment

Designation	Mean diameter[a] (μm)	Mean diameter[b] (μm)
SG	3.3	4.1
LG	24.4	27.9

[a] Mean diameter obtained using a particle size analyzer [26–28].
[b] Mean diameter obtained using an optical microscope [26–28].

and the size does not exist. Furthermore, some micro-mechanical deformation mechanisms occurring during crack propagation still remain undiscovered, as will be shown in this paper.

In this study, glass bead filled DGEBA (diglycidyl ether of bisphenol A)/DDS (4,4′-diaminodiphenylsulphone) epoxies are used to investigate the effects of volume fraction and size of glass beads on the fracture behavior of composites. A comprehensive investigation on the micro-mechanical deformations occurring during crack propagation will be performed using various microscopy techniques. In particular, the dependence of not only fracture toughness but also micro-mechanical deformations on the two material parameters will be studied. The result of this study will be an essential building block for establishing a more complete picture of underlying toughening mechanisms.

2. Experimental

2.1. Materials

To avoid any confusion of terminology, the word 'epoxide' will be used for low molecular weight, unreacted resins and 'epoxy' will mean the cured epoxy thermoset. The epoxide, DER 661® (M_w = 1750–1950), is a solid DGEBA resin produced by the Dow Chemical Co. DDS (98%), other solvents and reagents were obtained from Aldrich Chemical Co. and used without further purification. Glass beads are Spheriglass® A-glass beads (soda-lime) with no surface treatment from Potters Industry Co. Their designations and average diameters can be found in Table 1.

Distilled water was used for the cleaning of glass beads. First, the glass beads were dispersed in distilled water (glass beads/H_2O = 0.29 g/ml) under mechanical stirring at room temperature for 6 h, followed by filtration. After this cleaning procedure was repeated three times, the cleaned glass beads were dried under vacuum at 70°C for 12 h. Large aggregates were screened out using a 75 μm sieve (mesh size = 200).

2.2. Preparation of composites

Among various DGEBA epoxides, DER 661® was chosen because of its high viscosity to prevent glass beads from settling to the bottom of the mold during curing. Higher molecular weight epoxides can also prevent this settling problem, but their viscosities are too high to be mixed with more than 10 vol% glass beads. The epoxides melted at 160°C were first degassed under vacuum for about 1.5 h. They were then mixed for 1.5 h with glass beads and for 40 min with stoichiometric amounts of DDS. After mixing, the degassed mixture was poured into a preheated metal mold, vertically mounted in a convection oven and cured for 16 h at 160°C followed by 2 h at 200°C. The oven was then switched off and the cured resin was allowed to cool slowly to room temperature in the oven. The amount of glass beads in epoxy resins was changed from 0 to 30 vol%. The basic properties of glass beads and epoxy matrix (designation: 661) were given in Table 2.

2.3. Characterization

Optical retardation due to thermal residual misfit was measured following the standard photometric method [13] using the Olympus BH-2 optical microscope and a SONY color video CCD camera, DXC-151A (resolution = 768 × 493 pixels). The wavelength of light (λ) was controlled using a green filter ($\lambda \approx 577$–492 nm). Thin sections for this measurement were prepared by the petrographic thin-sectioning technique [14–16]. Samples were polished using silicon carbide (SiC) grinding discs (grit size 80, 250, 400, 600, 1000) and alumina suspensions (5, 1, 0.3, 0.05 μm). To reduce the influence of artifacts generated by polishing, sample thickness for this optical retardation measurement is rather greater (around 250 μm) than the thickness of other thin sections for optical microscopy (OM) investigation (usually around 40 μm). Only optical retardation at about $R/r_o = 1.15$ was measured with increasing temperature under an isotropic assumption, where R is the distance from the center of a glass bead and r_o is the radius of the glass bead. The assumption that the matrix is optically

Table 2
Physical properties of epoxy matrix materials and glass beads

Materials	Density (g/cm^3)	T_g (°C)	Modulus (GPa)	Yield stress (Mpa)	Solubiity parameter
661 (DER 661®/DDS)	1.204	124	2.8	88	11.5–13[a]
Glass beads (Spheriglass® A-glass beads)	2.5	Softening point = 704	70		

[a] From Ref. [84].

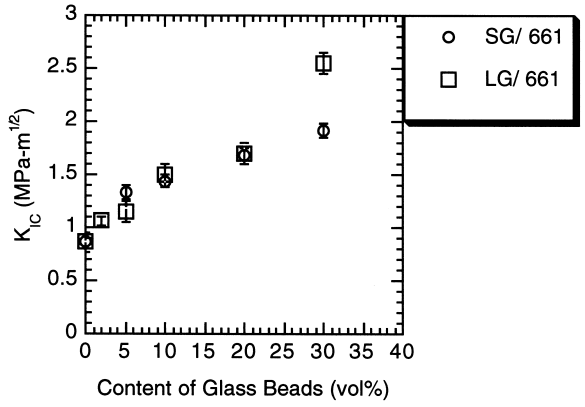

Fig. 1. Critical stress intensity factor versus glass bead content for glass bead filled epoxies.

isotropic has been previously used by other researchers [17–21].

Single-edge-notched (SEN) type specimens were prepared for the determination of the critical stress intensity factor (K_{IC}) in the three-point bend (3PB) geometry. Specimen thickness (B) and width (W) are 6.35 and 12.7 mm, respectively. This specimen geometry satisfies the requirement for the plane strain condition (ASTM E399), $B > 2.5(K_{IC}/\sigma_y)^2$, e.g. $B > 2.1$ mm for 30 vol% LG/661. For the preparation of a sharp notch in specimens, a razor blade was first immersed in liquid nitrogen until boiling stops, then it was inserted into specimens by tapping with a mallet. The sizes of all resulting initial cracks were longer than the insertion length of razor blades. This observation is important because, otherwise, the prepared initial crack tip may contain artifacts from the razor blades. Twelve to eighteen samples were tested on a screw-driven Instron machine (Instron 4502) at a crosshead speed of 2.54 mm/min using a span of 50.8 mm. Without any correction due to the length variation of an initial crack, the maximum length of an initial crack was used for K_{IC} calculation. The K_{IC} values were determined using the relationship [22,23]:

$$K_{IC} = Y\frac{3PS\sqrt{a}}{2BW^2}$$

$$Y = 1.93 - 3.07(a/W) + 14.53(a/W)^2 - 25.11\,(a/W)^3 + 25.80(a/W)^4 \quad (1)$$

where Y is a shape factor, P is the load at failure, S is the length of the span, and a is the crack length. Critical strain energy release rates (G_{IC}) were calculated from the stress intensity values using the following relationship [23,24]:

$$G_{IC} = \frac{K_{IC}^2}{E} \quad (2)$$

This relationship works only in plane stress conditions and true G_{IC} values in plane strain conditions for our systems can be obtained by multiplying by $(1-\nu^2)$, where ν is Poisson's ratio. Since the precise values of Poisson's ratio were not measured and the multiplicative factor cannot change the major results obtained from G_{IC} analyses in any significant way, G_{IC} values obtained from Eq. (2) were used in this study.

The fracture surface of SEN-3PB specimens was observed using a scanning electron microscope (SEM), a Hitachi S-800. Specimens were coated with a thin layer of gold-palladium to reduce charge build-up. The accelerating voltage was either 5 or 3 kV.

Sub-critically loaded cracks were obtained by using a double-edge-notched (DEN) specimen in the four-point bend (4PB) geometry following the same experimental technique developed by Sue and Yee [25]. Usually, two thin-sections were prepared and examined for each glass bead filled epoxy. Sub-surface damage in the process zone of a 3PB specimen was also assessed by using thin-sections taken from the specimen's mid-plane, perpendicular to the fracture surface.

Uniaxial tensile tests were also performed to measure the modulus of our composites (ASTM D 638). Samples were cut into small tensile specimens (gauge section = $15 \times 5 \times 7$ mm^3) and the specimens were polished using silicon carbide (SiC) grinding discs (grit size 80, 240, 400, 600) to remove surface defects. At least five specimens were tested for each composition. The same screw-driven Instron machine was used at a crosshead speed of 2.54 mm/min.

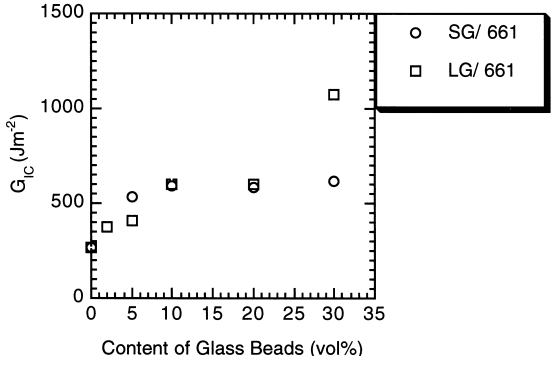

Fig. 2. Critical strain energy release rate versus glass bead content for glass bead filled epoxies.

3. Results and discussion

3.1. Mechanical properties of composites

Several basic characterizations on glass beads and filled composites were performed to verify our preparation method. Void contents in epoxy composites were found to be small, normally less than 1%. The glass transition temperature (T_g) of epoxy matrices in composites was found to be insensitive to the existence of glass beads. All

Table 3
Optimum content of glass beads in various experiments

Mean diameter of glass beads (μm)	Optimum content of glass beads[a] (vol%)	References
3.3	20	This experiment
4.5	30	[6]
16	30	[6]
24.4	>30	This experiment
32	40–46	[6]
47	>46	[6]
50.3	40	[10]
62	>46	[6]

[a] Optimum content where the K_{IC} of composites reaches a maximum value.

T_gs measured lie within 124 ± 2°C. Details of these experiments and others on the cleaning process and characterization of glass beads can be found elsewhere [26–29].

The fracture toughness, i.e. the critical stress intensity factor (K_{IC}), of glass bead filled epoxies is given in Fig. 1. In this figure, the error bar is the standard deviation for more than 12 measured values. The most distinctive feature in this figure is that the fracture toughness of two composite systems significantly increases with increasing glass bead content, which is quite consistent with previous research [3–6,8–12,30–32]. On the other hand, the size does not seem to be an important factor in determining the fracture toughness of composites. Only at 30 vol% glass bead content can the larger glass beads (LG) toughen epoxies significantly more than the smaller glass beads (SG). However, the size effect cannot be found at less than 30 vol%. These results can ensue from the detrimental effect of debonding, which is discussed in the following section.

The critical strain energy release rates (G_{IC}) calculated from the K_{IC} and modulus data can be found in Fig. 2. The general trend of this figure is the same as that of Fig. 1: fracture toughness increases with increasing glass bead content. Nonetheless, in all systems, as glass bead content increases, the increase of fracture toughness per unit increase of glass bead content becomes smaller more rapidly in Fig. 2 than in Fig. 1. This difference between K_{IC} and G_{IC} data can be easily understood by considering how they are related: G_{IC} depends on K_{IC} and modulus under the linear elastic fracture assumption (refer Eq. (2) and Refs. [6,7]).

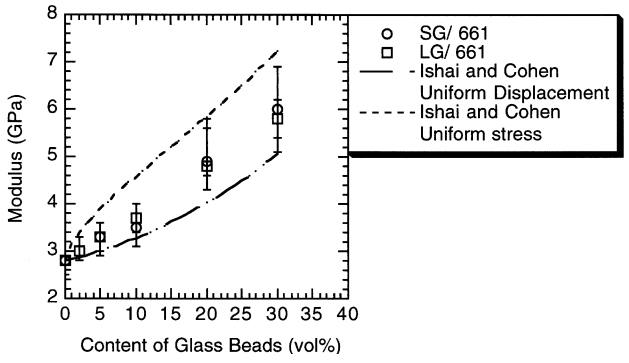

Fig. 3. Tensile modulus versus glass bead content for glass bead filled epoxies.

One interesting result can be obtained from previous work [6,7,10] and data shown here. In Table 3, the optimum contents of glass beads, where the fracture toughness of composites reaches a maximum value, are compared with respect to the sizes of glass beads. Although precise optimum contents are not always available, Table 3 shows that they generally increase as the size of glass beads increases. A possible explanation can be given as follows. As glass bead content increases, the inter-particle separation between glass beads becomes smaller and more and more glass beads can debond from the matrix. Microcracks generated by this debonding ahead of crack tips may act as defects facilitating crack propagation. Therefore, K_{IC} reaches a maximum value with increasing glass bead content. If the inter-particle separation becomes shorter, such as the case of smaller glass bead filled epoxies, the detrimental effect of microcracks could be larger, resulting in lower optimum contents of glass beads.

In typical microcracking toughening mechanisms [33–39], the generation of microcracks ahead of the crack tip is considered a beneficial event for toughening. However, if crack propagation is unstable and the orientation of most microcracks is parallel to the crack propagation direction like the case in our systems, the detrimental effect of microcracks could dominate over their beneficial effects, resulting in a decrease of fracture toughness.

Fig. 3 shows the moduli of composites prepared in the present experiment in which the range between the maximum and minimum values obtained from five different measurements for a composition is shown. First of all, the monotonic increase in modulus with the increase of glass bead content is obvious. No significant glass bead size effect on the modulus of composites can be found, in agreement with a previous study on silica filled epoxies [31,40–43]. On the other hand, other research [44–46] has demonstrated that the use of nano-silica particles can increase the modulus of composites more dramatically than that of micron-silica particles. The reason for this is not known now, but this finding gives strong motivation for the development of nanoparticle filled polymers, i.e. 'nanocomposites'. Probably, the reason why the size effect is not obvious in our results might be because the size difference between glass beads is too small to affect the modulus of composites.

There are many theoretical predictions to determine the moduli of filled composites. In Fig. 3, the theoretical prediction from the equations proposed by Ishai and Cohen [47] is compared with experimental values. The equations are derived from a two-phase model of a cubic matrix containing a cubic inclusion under two conditions.

Under the uniform stress condition:

$$\phi_f = \frac{E_c}{E_m} = \frac{1 + (m-1)C_f^{2/3}}{1 + (m-1)(C_f^{2/3} - C_f)} \quad (3)$$

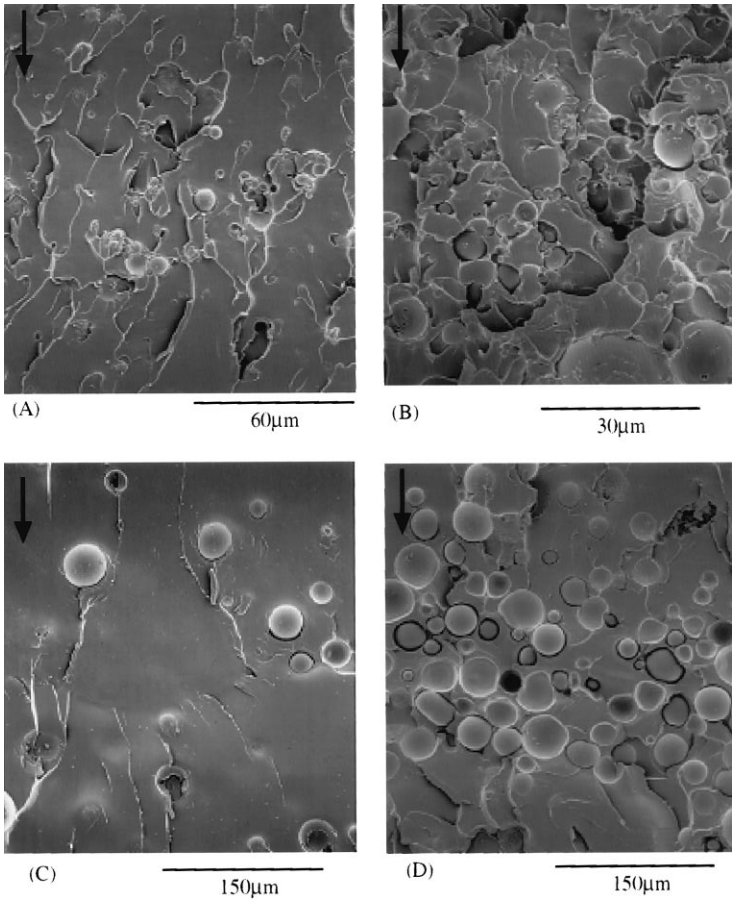

Fig. 4. SEM micrographs of the fracture surface (process zone) of SEN-3PB specimens: (A) 10 vol% SG/661; (B) 30 vol% SG/661; (C) 10 vol% LG/661; (D) 30 vol% LG/661. The arrows indicate the direction of crack propagation.

Under the uniform displacement condition:

$$\phi_f = 1 + \frac{C_f}{m/(m-1) - C_f^{1/3}} \quad (4)$$

where $m = E_f/E_m$, E_f modulus of filler, E_m modulus of matrix, E_c modulus of composite, and C_f volume fraction of filler. The predictions form upper and lower bounds to the experimental data.

3.2. Microscopy study I—SEM micrographs

The fracture surface of SEN-3PB specimens usually has three different regions: pre-crack, process zone, and fast-fracture region [14,48]. The pre-crack region is produced by the razor blade wedging open the crack. During the testing, cracks first undergo stable sub-critical growth in the process zone and subsequently to propagate unstably in the fast-fracture region. The process zones are usually examined to understand toughening mechanisms, because the materials' resistance against crack propagation in this region actually reflects the fracture toughness measured.

Fig. 4 shows process zones on the fracture surface of 10 and 30 vol% filled epoxies. Debonded glass beads are evident here. The existence of debonded glass beads makes process zone size measurable using SEM. (The process zone size in here is essentially equivalent to the debonding zone size.) In Fig. 4(A) and (C), the process zone is confined in a very small area (in the middle of the micrographs), where glass beads are partially or fully debonded. In this case, the process zone is almost a line. As the volume fraction of glass beads increases (Fig. 4(B) and (D)), the process zone size increases too. In all other investigations on fracture surface, it was generally found that debonding zone size increases with an increase in glass bead content. Besides debonded glass beads, crater structures are also evident in Fig. 4. This was formed after the glass beads were pulled out of the epoxy matrix. Around debonded glass beads, there are gaps. They may have resulted from the plastic dilatation of the matrix, which occurred after the initiation of debonding.

Behind the glass beads in Fig. 4, there are characteristic tail structures [6,7,49], which are in reality steps on the fracture surface. These are formed when two secondary crack fronts divided by a glass bead meet with each other. Usually, the crack propagation planes of secondary cracks cannot be perfectly coplanar. In addition to the tail structures, similar structures [50–57], e.g. rivers, hackles, and

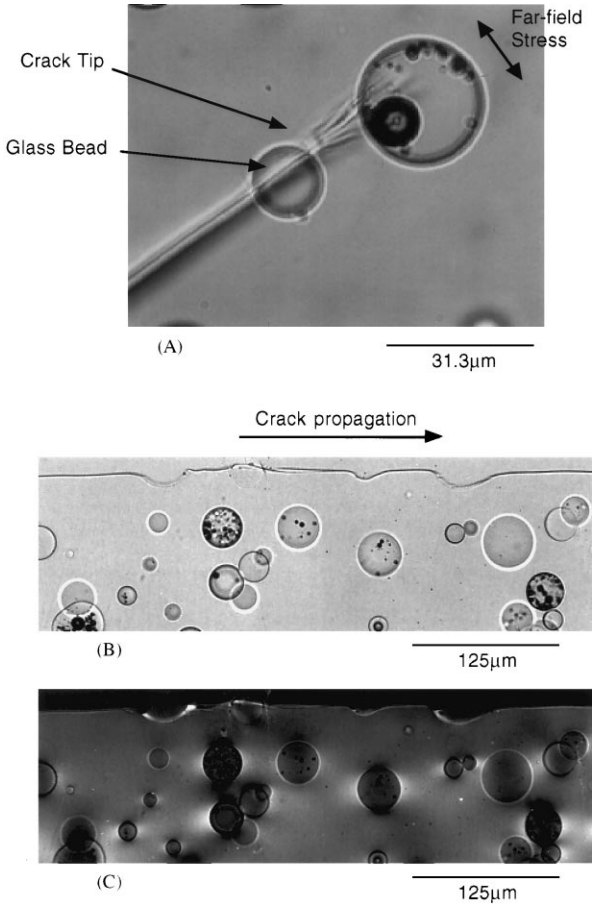

Fig. 5. Transmitted light optical micrographs of thin sections of 10 vol% LG/661: (A) tip of a sub-critically loaded crack in a DEN-4PB specimen; (B) process zone in a SEN-3PB specimen (without polarizers); (C) the same region as that in (B), but between crossed polarizers.

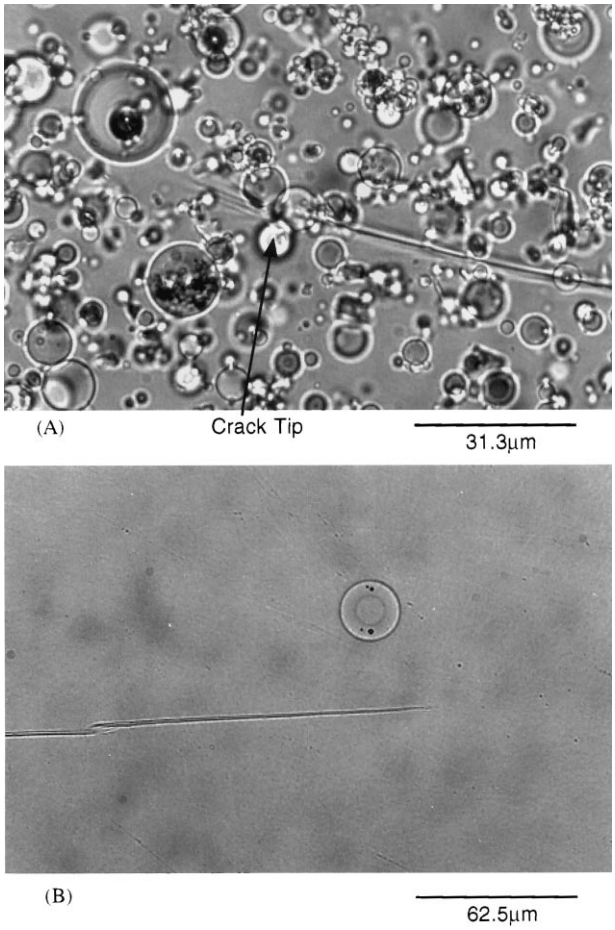

Fig. 6. Transmitted light optical micrographs of thin sections taken near the tip of sub-critically loaded cracks in DEN-4PB specimens: (A) 10 vol% SG/661; (B) 2 vol% LG/661.

lances, can also be found on the fracture surface. These can be categorized with the tail structure into *steps*, because their features on the fracture surface are similar. However, they are formed for different reasons independently of the existence of glass beads, such as mixed mode stress states in constrained specimen geometry and local fluctuation of stress distribution, etc. [51–54,58].

Fig. 4 shows that, compared to the 10 vol% glass bead filled systems, 30 vol% glass bead filled epoxies have more steps per unit area, whose directions are more irregular. This can be easily understood, because more steps can be formed by debonding of glass beads as glass bead content increases. Debonding ahead of crack tips always produces isolated secondary cracks, which have different crack propagation directions from the primary crack propagation direction. When the primary and the isolated secondary crack fronts (or two isolated secondary crack fronts) meet with each other, randomly directed step structures will be formed in the process zones.

At the same glass bead content, there are fewer steps per unit area of fracture surface in large glass bead systems than in small glass bead systems (Fig. 4). This size effect on step formation is not unexpected. If glass bead size increases, the number of glass beads per unit fracture surface area will decrease, so the number of secondary cracks per unit area generated by debonding of glass beads ahead of crack tips will decrease also. Consequently, this series of events will cause the number of steps per unit area to decrease.

3.3. Microscopy study II—OM micrographs

In the fracture toughness tests of SEN-3PB specimens, the typical load–displacement curves of glass bead filled epoxies were as linear as those of unfilled (neat) epoxies. This linearity indicates that the fracture of glass bead filled epoxies is very brittle. Therefore, it can be expected that sub-surface damage is not extensive and insignificant compared to surface damage, which researchers usually focused on. However, in the present experiment, possible sub-surface damages are thoroughly investigated.

Figs. 5–8 shows the sub-surface damage in sub-critically loaded and fractured specimens. Before this sub-surface damage is discussed, possible artifacts due to the preparation of thin-sections must be identified. The circles in the

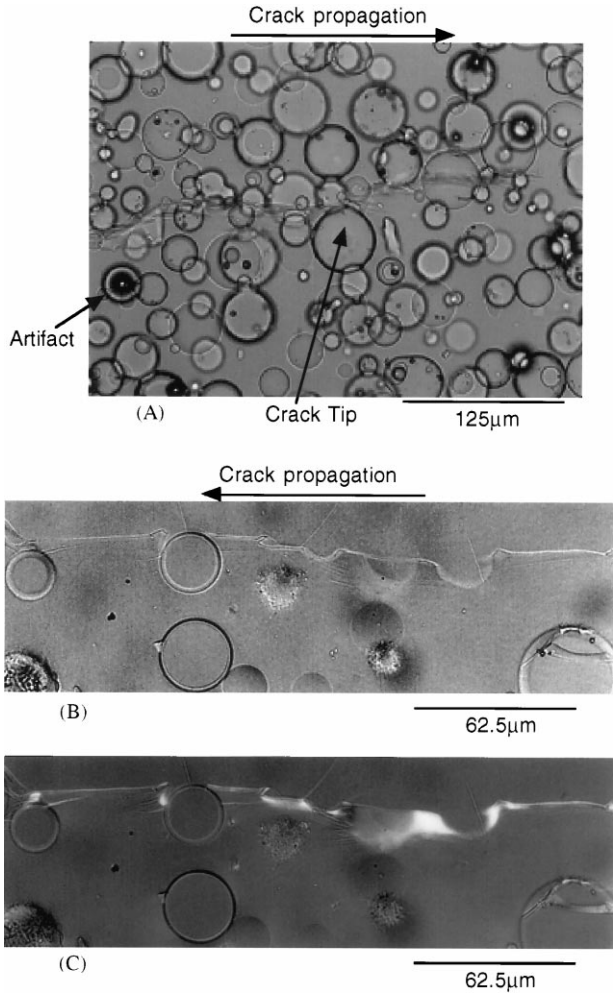

Fig. 7. Transmitted light optical micrographs of thin sections of 30 vol% LG/661: (A) tip of a sub-critically loaded crack in a DEN-4PB specimen; (B) process zone in a SEN-3PB specimen (without polarizers); (C) the same region as that in (B), but between crossed polarizers.

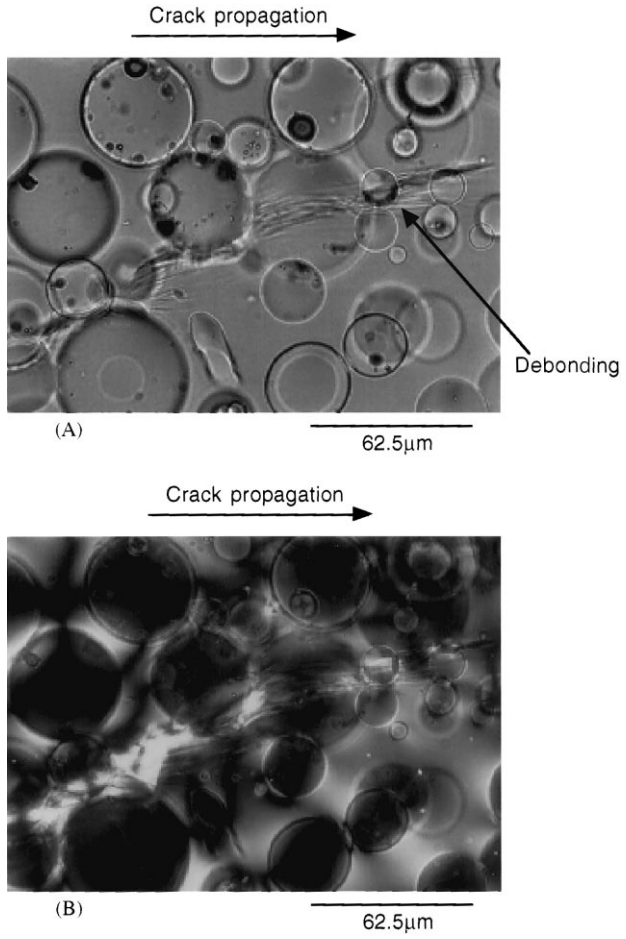

Fig. 8. Transmitted light optical micrographs of thin sections taken near the tip of a sub-critically loaded crack in a DEN-4PB specimen of 30 vol% LG/661: (A) without polarizers; (B) the same region as that in (A), but between crossed polarizers.

OM micrographs of thin-sections are glass beads, and small dark spots frequently found inside these circles are usually small dust particles on the polished surface of thin-sections. This was confirmed by examinations using reflected light. These particles could be broken glass bead fragments or just alumina particles from polishing. Occasionally, the glass bead in these micrographs appears to be a set of alternating dark and bright concentric rings (Fig. 7(A) Artifact). These glass beads can be found frequently in polished thin-sections. These were debonded by polishing and usually lie near the surface of thin-sections. The rings result from optical interference [59] due to the air gap between the debonded glass beads and the matrix. This will be further discussed later. The existence of concentric rings indicates that debonding is initiated from a point on the glass bead surface closest to or farthest away from the polished surface of thin-sections. On the other hand, debonding due to the loading of fracture tests produces asymmetric dark regions in OM micrographs, because debonding starts from the interface normal to the loading direction (pole region) which is parallel to the surface of thin-sections (Fig. 8(A) Debonding).

Fig. 5(A) shows the sub-critically loaded crack tip of 10 vol% LG/661. The tip is forked into several fine dark lines. We have ascertained that these fine lines are micro-shear bands [60–62]. This is shown by two different experiments. First, by using SEM and TEM, it was found that no cracks or crazes exist around the sub-critically loaded crack tips of all the specimens cryofractured and microtomed perpendicular to the crack propagation planes. Thus, these dark lines are not due to the existence of cracks or crazes. Second, heating the thin-sections up to the T_g of the epoxy matrix caused the dark lines to disappear at a temperature below the T_g of the matrix. Crack healing in thermosets is unlikely to occur at this temperature. More experimental details and results can be found elsewhere [26–29].

Micro-shear bands are also found to be visible in the thin-sections of fractured SEN-3PB specimens. However, the micro-shear bands in Fig. 5(B) and (C) are not easily discernible, mainly because the magnification of these

micrographs is relatively low. These micrographs are chosen to show the diffuse shear yielded region of matrix around the crater. The birefringence of the shear yielded zone is noticeable in (C), a micrograph taken between crossed polarizers. Diffuse shear yielding is found in the matrix around all debonded particles in the process zones, regardless of the volume fraction or size of the glass beads.

Fig. 5 also shows that the near equatorial region of the crater is more birefringent than the other parts. (The equatorial region refers to the interfacial region between glass beads and the matrix, which is parallel to the direction of the far-field stress. Thus, the far-field stress is along the poles.) This is generally found in all diffuse shear yielded regions around craters. When a plate having a through hole undergoes loading, it is well known that the maximum von Mises stress is found around the equatorial part of the hole [24,63–66]. In glass bead filled epoxies, after a glass bead debonds, the resulting crater region is less geometrically constrained, so it can start to yield from its equatorial region where the stress concentration is the highest. Therefore, the more birefringent equatorial region, found in Fig. 5, seems to be a reasonable result. Even if the shear yielding occurs due to the mixed mode crack propagation along the interface between glass beads and matrix, the more birefringent equatorial region will result, because the crack propagation in this region has higher mode II or mode III components [64,67–69].

Fig. 6 shows the sub-critically loaded cracks of a SG system (10 vol% SG/661) and a low LG content system (2 vol% LG/661). In (A), it is obvious that micro-shear bands are developed from a glass bead at the crack tip. The glass bead at the crack tip also has a dark region indicating the debonding of the glass bead. On the whole, there are not many differences between the micrographs of SG and LG systems (Figs. 5(A) and 6(A)), except for a slightly smaller micro-shear band zone and a significant aggregation in SG systems. (Further discussion on the effect of aggregation can be found in Refs. [26–29].) One difficulty in the examination on small glass bead systems is that too many glass beads exist in a thin-section, which can obscure the micro-deformations. As glass bead content increases, this screening becomes more severe and observation on micro-deformations more difficult. To avoid this screening effect, thin-sections containing a small number of glass beads, i.e. only one or two layer(s) of SG, must be prepared. Consequently, the thickness of thin-sections must be less than 10 μm, which is almost impossible to obtain in reality using the petrographic thin-sectioning technique [14–16].

Fig. 6(B) shows a sub-critically loaded crack tip of 2 vol% LG/661. In the crack path, a ‘lance’, a kind of step, is visible [50,53]. Because the glass bead content of this specimen is only 2 vol%, only one glass bead is captured in the micrograph (B). The features around the sub-critically loaded crack tip of this micrograph are the same as those around the tips of unfilled (neat) epoxies. On the basis of several decades of research on the fracture of neat epoxies, it is now generally believed that localized shear yielding at crack tips is the major micro-mechanical deformation during crack propagation in neat epoxies [4]. The crack propagation in the epoxies filled with a small amount of glass beads may mostly occur in the same manner as that in unmodified epoxies. Since no micro-shear banding and debonding of glass beads can be found in Fig. 6(B), the glass bead in this micrograph does not seem to have any significant influence on the micro-deformations of crack propagation.

If a glass bead is at the crack tip (crack arrest line) of 2 vol% LG/661, it may debond and generate a diffuse shear yielded region, or generate micro-shear bands. In fact, the probability of preparing a thin-section containing a glass bead at the crack tip is extremely low, when glass bead content is only 2 vol%. In this case, the average inter-particle distance between glass beads (D_i) is about 600 μm. If glass bead content is 10 vol%, D_i is about 150 μm. Therefore, among the thin-sections of 10 vol% LG/661, some do not contain glass beads at crack tips because the section is thinner than 150 μm. In these thin-sections, micro-shear bands are found to be almost invisible or smaller than in the thin-sections containing a glass bead at the crack tip (Fig. 5(A)). This suggests that micro-shear bands exist only in the vicinity of the glass beads at the crack tip (or in the crack path).

Figs. 7 and 8 show the OM micrographs for 30 vol% LG/661 composites. It can be found in these micrographs that micro-shear bands are well developed between glass beads. Accordingly, a large zone containing micro-shear bands forms ahead of the crack tip. The size of this zone is found to increase as glass bead content increases [26–29]. Besides the micro-shear bands, crack deflection or step structures can be found in Figs. 7 and 8. One possible inference from these micrographs is that a crack may propagate (deflect) from glass bead to glass bead through one of the fully developed micro-shear bands between the glass beads.

Figs. 7 and 8 also show the debonding of glass beads and the diffuse shear yielding of the matrix. In Fig. 8, the dark regions inside glass beads directly indicate the debonding of glass beads. As discussed above, they result from the interference of light in the gap between debonded glass beads and matrix. If these rings are examined under reflected light, dark rings under transmitted light become bright and bright rings become dark [59]. Since visible light is used, the approximate thickness of the gap which can effectively enable the interference to occur is 0.3–1.4 μm. In addition to interference, light scattering can be a reason why the debonded region appears dark in the micrographs. In the SEM micrographs, drawn fibrils of the matrix were found between partially debonded glass beads and matrix [26–29]. These complicated structures can effectively scatter visible light and make this debonded region appear dark in the micrographs. This effect will disappear after the drawn structures of matrix break down with progress in debonding.

Diffuse matrix shear yielding is also noticeable in Figs. 7

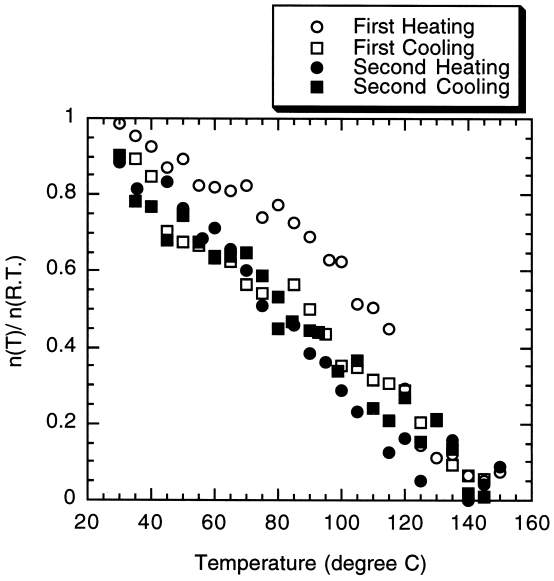

Fig. 9. Optical retardation around a glass bead, $n(T)$, during repeated heating and cooling at 1°C/min in a thin section (thickness = 320 μm) of 5 vol% LG/661. The n(R.T.) is initial optical retardation at room temperature before this test.

and 8. The birefringence of diffuse shear yielded regions around the glass beads in the process zone is stronger than the birefringence of the thermal residual misfit, which will be discussed later. Because diffuse shear yielding is always found around the debonded matrix, it is natural to surmise that the debonding of glass beads initiates the diffuse matrix shear yielding. Once a glass bead debonds from the matrix, a free surface will be generated, which is more vulnerable to plastic shear deformation. Although this explanation seems reasonable, another explanation can also be given. Since the interfacial failure between glass beads and matrix is not pure mode I fracture, plastic shear yielding can be enhanced by the mixed mode stress conditions. Nevertheless, a careful investigation of Figs. 7 and 8 reveals that diffuse shear yielding can be found even when the mixed mode component is insignificant. Consequently, the first explanation is more likely than the second.

3.4. Thermal residual misfit

In addition to the relatively strong birefringence around craters, weak birefringence can be found around all glass beads (Figs. 5(C) and 8(B)); This is the birefringence due to residual misfit stress (or strain) [17,18,70–72]. The residual misfit can be generated by two possible reasons. One is the differential thermal contractions of glass beads and matrix during cooling from the curing temperature. The discrepancy between coefficients of thermal expansion (CTE) of two materials is large enough to cause significant stress to develop around glass beads [17–21,70,71]. The linear CTE of glass beads is $3–5 \times 10^{-6}$ ($°C^{-1}$) [73] and that of typical epoxy resins is about $50–80 \times 10^{-6}$ ($°C^{-1}$) [73]. The other possible reason is the shrinkage of epoxy resins during its curing [74–76].

To examine the nature of the weak birefringence around glass beads, optical retardation measurements [13] with changing temperature was attempted. If linear photoelasticity [13,77] is valid in our systems, relative optical retardation (n) can be directly converted into misfit stress:

$$n = \frac{Cd}{\lambda}(\sigma_1 - \sigma_2) \qquad \text{for two-dimensional systems} \qquad (5)$$

where λ is the wavelength of light, C is the stress-optical constant of materials, d is sample thickness, and σ_1 and σ_2 are the principal stresses. Since it is not known whether plasticity and viscoelasticity play a significant role or not, the conversion of optical retardation into misfit stress was not tempted. Only the optical retardation data normalized by the optical retardation at room temperature around a glass bead is obtained upon repeated heating and cooling. Such data are plotted in Fig. 9. The use of normalized values can minimize any possible artifacts introduced by optical elements, thin-sectioning, and noise in image digitization. Repeated experiments proved that our measurement gives reproducible (and most likely reliable) data for normalized optical retardation.

Fig. 9 reveals that the birefringence can be removed by heating the composites above the T_g of the matrix (124°C). Most birefringence disappears at about 140°C, as one would expect of the residual misfit as well. More interestingly, when the heated sample is cooled down to room temperature, most birefringence reappears (Fig. 9), although there is a slight hysteresis between heating and cooling curves. Since the curing temperature of the composites is above 140°C and the relaxation of matrix at this temperature is rapid, the curing shrinkage of the epoxy matrix could not build up any significant misfit birefringence at this temperature. Accordingly, cooling from the curing temperature is likely to be the main source for the misfit birefringence noticeable at room temperature.

This experiment is important, because the examination on the nature of misfit birefringence in filled composites has rarely been reported [75,76] and, furthermore, there is a report [78] showing that the misfit birefringence cannot be removed by heating. Removing misfit birefringence is nothing but a problem of the competition between the relaxation of matrix and the amount of misfit developed in composites. If heating is relatively fast, birefringence may remain above T_g of matrix for a certain period of time. In our experiments, when thin-sections were heated at 10°C/min, a significant amount of birefringence persisted even after the temperature passed 140°C. This time sensitive behavior was also observed when thin-sections free of birefringence at 140°C were cooled down to room temperature at different cooling rates: as the cooling rate increases, the misfit birefringence increases. These results show that the thermal residual misfit stress (or strain) cannot be calculated directly from CTE values because of its viscoelastic nature.

Several previous reports provide quantitative estimates of the thermal residual misfit stress in glass bead filled epoxies obtained by theoretical calculations or experimental measurements [17–21,79]. However, large discrepancies can be readily found among the data sets. Furthermore, most reports assume linear elastic behavior of the materials, which is not true in polymers. Fortunately, the absolute value of thermal residual stress is not our major concern, rather it is whether the thermal residual misfit can affect the fracture toughness of composites and, if it can, how much its contribution is.

The effect of thermal residual misfit on fracture toughness can be assessed by examining the possible mechanisms that can link misfit stress with fracture toughness. The thermal residual misfit in glass bead filled epoxies can cause tensile hoop stress and compressive radial stress to develop around glass beads, because the CTE of glass beads is smaller than that of the matrix [80]. The tensile hoop stress can promote annular microcracking around glass beads ahead of the crack tip [24,81]. However, no evidence for these annular microcracks was found in any of the micrographs. The compressive radial stress can increase the interfacial strength between glass beads and matrix. Through the variation of interfacial strength, the fracture toughness of composites might be affected by the thermal residual misfit. However, this effect of thermal residual misfit must be quite small because the effect of interfacial strength on the fracture toughness of composites is found to be insignificant in the previous [6,7,9,82,83] and our studies [26–29].

As another approach to answering the questions, possible interactions between the misfit birefringence and crack tip stress field were examined. As can be seen in Figs. 5 and 8, crack propagation cannot significantly change the misfit birefringence around most glass beads. Only the misfit birefringence around the glass beads very close to the crack path is significantly altered by the crack tip stress or crack propagation. Thus, the influence of thermal residual misfit on the fracture toughness of composites can hardly be expected to be extensive.

4. Conclusions

A systematic investigation has been performed on the fracture process of glass bead filled epoxy resins by changing the volume fraction and size of glass beads. From microscopy studies on fractured and sub-critically damaged specimens, several micro-deformation mechanisms occurring during crack propagation were identified: step formation on fracture surface, debonding of glass beads, diffuse matrix shear yielding, and micro-shear banding. The debonding of glass beads was found to be usually accompanied by diffuse matrix shear yielding which can be initiated by debonding. Micro-shear bands were thought to be initiated and propagated from glass beads at the crack tip region.

Increasing the volume fraction of glass beads resulted in a successful improvement in the fracture toughness of composites. However, it was found that the toughening effect of glass beads (the increase of fracture toughness per unit increase of glass bead content) decreased as glass bead content increased. With increasing glass bead content, the modulus of composites was found to increase. The increase of debonding zone size, micro-shear band zone size, and the number of steps per unit area were noticed as glass bead content increased. The fracture toughness and tensile modulus of composites was shown to not significantly depend on the size of glass beads. Microscopy studies on the fracture surface demonstrated that smaller glass bead systems had more steps per unit area than larger glass bead systems.

In addition to the relationship between micro-deformation mechanisms and crack propagation, birefringence due to misfit stress (or strain) was also studied. Optical retardation experiments demonstrated that birefringence was caused mainly by the differential thermal contractions of glass beads and the matrix, not by the curing shrinkage of matrix under the present curing conditions. The development of thermal residual misfit was found to be time sensitive, so it had viscoelastic or plastic natures. Microscopy studies showed that the interactions between the crack tip stress and the thermal residual misfit stress was not extensive.

Acknowledgements

This work was supported by the Specialized Materials Science Research Center of National Institute of Health (NIH), under a contract No. DEO 9296-09. The authors would like to thank Dr Hajime Kishi, Dr Jack Huang and Ms Jacqueline M. Denoyer for their help.

References

[1] Craig RG. Restorative dental materials, 8th ed. St. Louis: Mosby, 1989.
[2] Stannard JG. Materials in dentistry. 2nd ed. Hanover: Denali, 1988.
[3] Rothon R. Particulate-filled polymer composites. New York: Longman, 1995.
[4] Kinloch AJ, Young RJ. Fracture behavior of polymers. Amsterdam: Elsevier, 1985.
[5] Nielsen LE, Lande RF. Mechanical properties of polymers and composites. 2nd ed. New York: Marcel Dekker, 1994.
[6] Spanoudakis J, Young RJ. J Mater Sci 1984;19:473.
[7] Spanoudakis J, Young RJ. J Mater Sci 1984;19:487.
[8] Young RJ, Beaumont PWR. J Mater Sci 1977;12:684.
[9] Moloney AC, Kausch HH, Stieger HR. J Mater Sci 1983;18:208.
[10] Kinloch AJ, Maxwell DL, Young RJ. J Mater Sci 1985;20:4169.
[11] Lange FF, Radford KC. J Mater Sci 1971;6:1197.
[12] Mallick PK, Broutman LJ. Mater Sci Engng 1975;18:63.
[13] Kuske A, Robertson G. Photoelastic stress analysis. New York: Wiley, 1974.
[14] Pearson RA, Yee AF. J Mater Sci 1986;21:2475.
[15] Holik AS, Kambour RP, Hobbs SY, Fink DG. Microstruct Sci 1979;7:367.

[16] Sawyer LC, Grubb DT. Polymer microscopy. New York: Chapman and Hall, 1987.
[17] Wang H, Li S, Yu T. Polym Engng Sci 1993;33:474.
[18] Wang H, Li S, Zhou H, Yu T, Jin X. Polym Engng Sci 1992;32:678.
[19] Pawlak A, Galeski A. Optical Engng 1995;34:3398.
[20] Pawlak A, Galeski A. Polym Engng Sci 1996;36:2727.
[21] Pawlak A, Galeski A. Polym Engng Sci 1996;36:2736.
[22] Brown WF, Srawley JE. ASTM STP 1965;381:13.
[23] Hertzberg RW. Deformation and fracture mechanics of engineering materials. New York: Wiley, 1989.
[24] Matonis VA, Small NC. Polym Engng Sci 1969;9:90.
[25] Sue HJ, Yee AF. J Mater Sci 1993;28:2975.
[26] Lee J. PhD thesis, The University of Michigan, 1998.
[27] Lee J, Yee AF. In preparation.
[28] Lee J, Yee AF. Polym Prepr, Am Chem Soc Div Polym Chem 1997;38:369.
[29] Lee J, Yee AF. Polym Prepr, Am Chem Soc Div Polym Mater 1998;79:200.
[30] Srivastava VK, Shembekar PS. J Mater Sci 1990;25:3513.
[31] Nakamura Y, Yamaguchi M, Okubo M, Matsumoto T. Polymer 1991;32:2221.
[32] Nakamura Y, Yamaguchi M, Okubo M. Polym Engng Sci 1993;33:279.
[33] Evans AG, Faber KT. J Am Ceram Soc 1983;67:255.
[34] Evans AG, Williams S, Beaumont PWR. J Mater Sci 1985;20:3668.
[35] Evans AG, Fu Y. Acta Metall 1985;33:1525.
[36] Rose LRF. J Am Ceram Soc 1986;69:212.
[37] Hutchinson JW. Acta Metall 1987;35:1605.
[38] Ortiz M. J Appl Mech 1987;54:54.
[39] Gao F, Wang T. J Mater Sci Lett 1990;9:1409.
[40] Nakamura Y, Yamaguchi M, Okubo M, Matsumoto T. Polymer 1991;32:2976.
[41] Nakamura Y, Yamaguchi M, Okubo M, Matsumoto T. Polymer 1992;33:3415.
[42] Nakamura Y, Yamaguchi M, Okubo M, Matsumoto T. J Appl Polym Sci 1992;44:151.
[43] Nakamura Y, Yamaguchi M, Okubo M, Matsumoto T. J Appl Polym Sci 1992;45:1281.
[44] Huang H, Wilkes GL, Carson JG. Polymer 1989;30:2001.
[45] Abramoff B, Covino J. J Appl Polym Sci 1992;46:1785.
[46] Landry CJT, Coltrain BK, Landry MR, Fitzgerald JJ, Long VK. Macromolecules 1993;26:3702.
[47] Ishai O, Cohen LJ. Int J Mech Sci 1967;9:539.
[48] Yee AF, Pearson RA. J Mater Sci 1986;21:2462.
[49] Lange FF. Phil Mag 1970;22:983.
[50] Sommer E. Engng Fracture Mech 1969;1:539.
[51] Atsuta M, Turner DT. J Mater Sci 1982;1:167.
[52] Kinloch AJ, Gilbert D, Shaw SJ. Polym Comm 1985;26:290.
[53] Purslow D. Composites 1986;17:289.
[54] Hull D. Int J Fracture 1993;62:119.
[55] Hull D. Int J Fracture 1995;70:59.
[56] Hull D. J Mater Sci 1996;31:1829.
[57] Hull D. J Mater Sci 1996;31:4483.
[58] Melin S. Int J Fracture 1983;23:37.
[59] Hecht E. Optics. Reading, MA: Addison-Wesley, 1987.
[60] Argon AS, Andrews RD, Godrick JA, Whitney W. J Appl Phys 1968;39:1899.
[61] Bowden PB, Raha S. Phil Mag 1970;25:463.
[62] Bowden PB. Phil Mag 1970;25:455.
[63] Goodier JN. J Appl Mech 1933;55:A39.
[64] Williams JG. Fracture mechanics of polymers. 1st ed.. Chichester, UK: Ellis Horwood, 1984.
[65] Broutman LJ, Agarwal BD. Polym Engng Sci 1974;14:581.
[66] Ricco T, Pavan A, Danusso F. Polym Engng Sci 1978;18:774.
[67] Faber KT, Evans AG. Acta Metall 1983;31:565.
[68] Kim HS, Ma P. Key Engng Mater 1998;137:179.
[69] Wang JS, Suo Z. Acta Metall 1990;38:1279.
[70] Chow TS, Wilson JC. J Polym Sci B 1978;16:967.
[71] Evans AG. J Mater Sci 1974;9:1145.
[72] Fan CF, Hsu SL. J Polym Sci B 1992;30:603.
[73] Mallick PK. Fiber-reinforced composites. New York: Marcel Dekker, 1993.
[74] Shimbo M, Ochi M, Shigeta Y. J Appl Polym Sci 1981;26:2265.
[75] Srivastava AK, White JR. J Appl Polym Sci 1984;29:1241.
[76] Srivastava AK, White JR. J Appl Polym 1984;29:2155.
[77] Dally JW, Riley WF. Experimental stress analysis. New York: McGraw-Hill, 1965.
[78] Shuster M, Sherman D, Siegman A, Narkis M, Juennewein CM, Eyerer P. Polym Composites 1996;17:568.
[79] Koh S, Kim J, Mai Y. Polymer 1993;34:3446.
[80] Clyne TW, Withers PJ. An introduction to metal matrix composites. New York: Cambridge University Press, 1993.
[81] Azimi HR, Pearson RA, Hertzberg RW. Polym Engng Sci 1996;36:2352.
[82] Sahu S, Broutman LJ. Polym Engng Sci 1972;12:91.
[83] Broutman LJ, Shau S. Mater Sci Engng 1971;8:98.
[84] Bucknall CB, Partridge IK. Polym Engng Sci 1986;26:54.